Re-assesment of proton radii from electron scattering

Vladyslava Sharkovska (PSI & UZH)

in collaboration with

F. Hagelstein, V. Lensky and V. Pascalutsa (JGU)

Status Proton Charge Radius

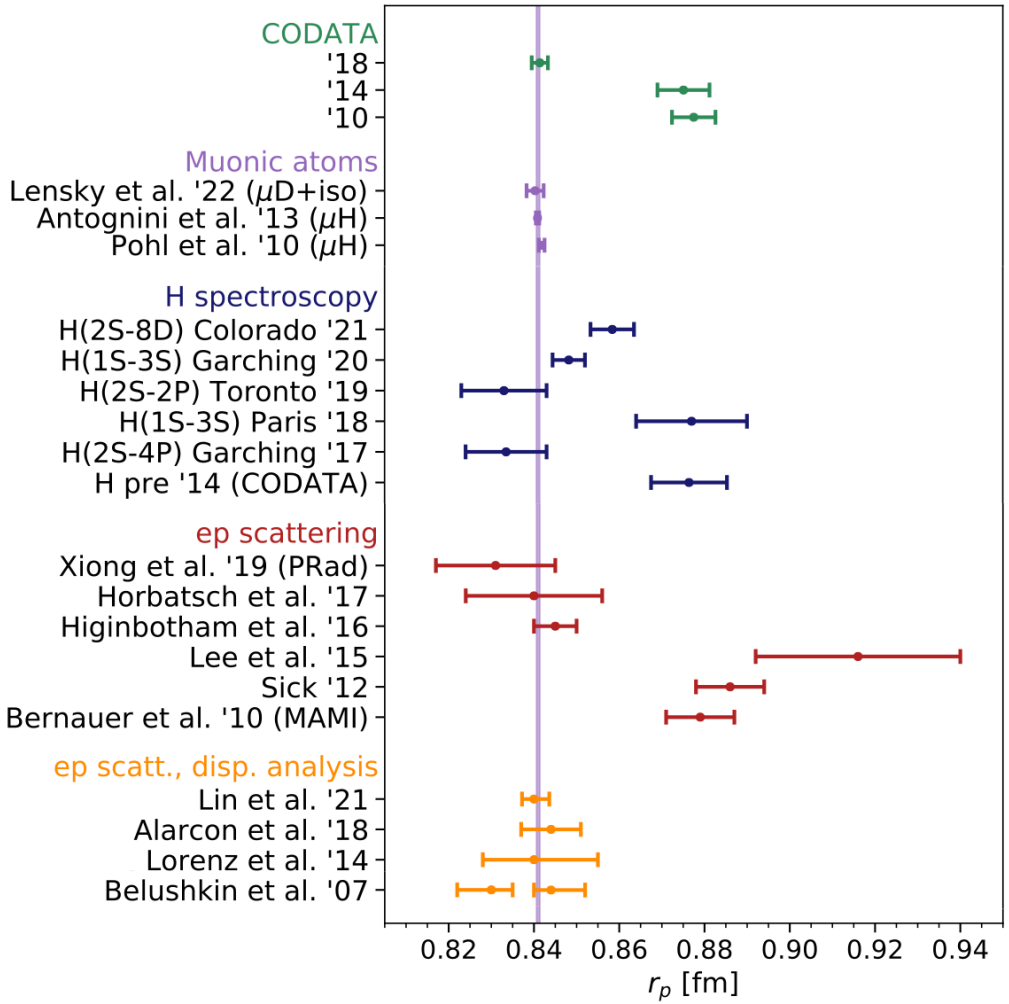

- Complementary experimental approaches:

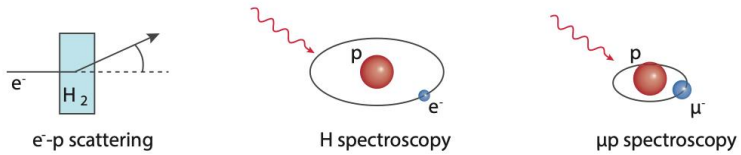

- Muonic atoms allow for PRECISE extractions of nuclear charge radii
- CODATA since 2018 included the μH result for r_p
- Still open issues: H(2S-8D), H(1S-3S) @ Paris
- Important question:

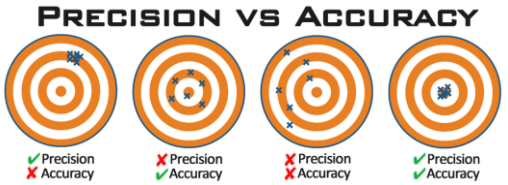

Why Muonic Atoms?

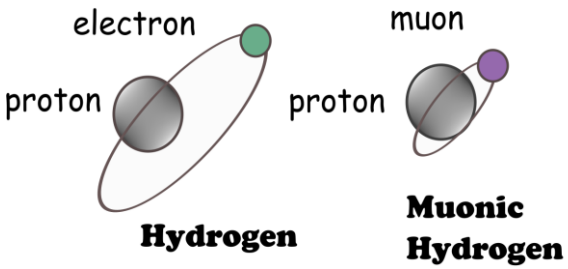

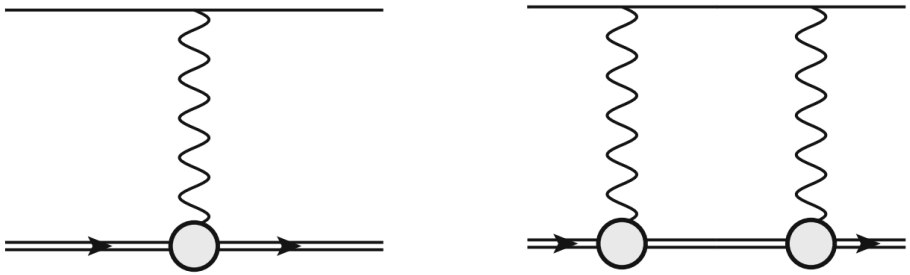

- **Lamb shift:**

wave function at the origin

charge radius

Friar radius or 3rd Zemach moment

$$\Delta E_{nl}(\mathrm{LO+NLO}) = \delta_{l0}\,\frac{2\pi Z\alpha}{3}\,\frac{1}{\pi(an)^3}\left[R_E^2 - \frac{Z\alpha m_r}{2}R_{E(2)}^3\right]$$

NLO becomes appreciable in μH

- **HFS:**

$$\Delta E_{nS}(\mathrm{LO+NLO}) = E_F(nS)\left[1 - 2\,Z\alpha m_r\,R_Z\right]$$

Zemach radius

Fermi - Energy:

$$E_F(nS) = \frac{8}{3}\frac{Z\alpha}{a^3}\frac{1+\kappa}{mM}\frac{1}{n^3}$$

with Bohr radius $a = 1/(Z\alpha m_r)$

Talk Outline

1. More accurate (not necessarily more precise) constraints on proton radii from electron scattering

2. More accurate (less model-dependent) input from electron scattering for muonic hydrogen spectroscopy

3. Survey of constraints on proton radii from scattering, spectroscopy, lattice QCD

Electric and Magnetic Form Factors

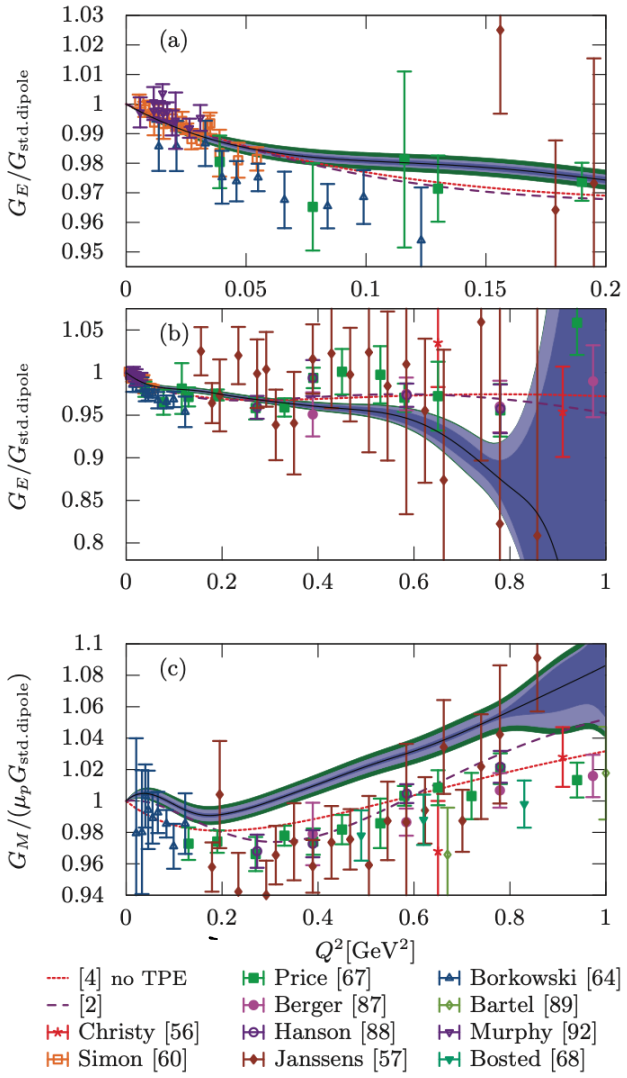

J. C. Bernauer *et al.*, Phys. Rev. C **90**, 015206 (2014)

- Measured in lepton-proton scattering
- Form factors (FF): Fourier transforms of charge and magnetization distributions

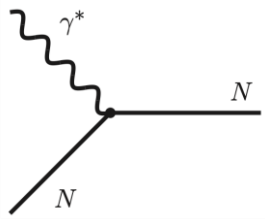

$$\Gamma_\mu = \gamma_\mu F_1(Q^2) + \frac{i}{2M}\sigma_{\mu\nu}q^\nu F_2(Q^2)$$
$$G_M(Q^2) = F_1(Q^2) + F_2(Q^2),$$
$$G_E(Q^2) = F_1(Q^2) - \frac{Q^2}{4M^2}F_2(Q^2)$$

$$\rho(r) = \int \frac{\mathrm{d}\boldsymbol{q}}{(2\pi)^3} G(\boldsymbol{q}^2) e^{-i\boldsymbol{q}\boldsymbol{r}}$$

- Root-mean-square (rms) radii of the proton:

$$R = \sqrt{\langle r^2 \rangle}$$
$$\langle r^2 \rangle \equiv \int \mathrm{d}\mathbf{r}\, r^2\, \rho(r) = -\frac{6}{G(0)} \frac{\mathrm{d}}{\mathrm{d}Q^2} G^2(Q^2)\Big|_{Q^2=0}$$

Overview of Electron Scattering data

Observables to be included as constraints for the proton form factors

1. Unpolarized cross section: **1** (A1) +**32** experiments, total of **2055** points

2. Polarization transfer: **14** experiments, total of **69** points

3. Initial state radiation extraction: **1** (MAMI) experiment, **25** points

A1 dataset:

- **1422** cross section points in the range of Q^2 € ~ [0.004, 0.977] GeV^2 and the range of ε € [0.06, 0.96]
- **72** points from Rosenbluth separation, in the range of Q^2 € ~[0.02, 0.55] GeV^2
- **34** spectrometer settings (subsets) with **31** independent normalization parameters
- Currently treated by us with **34** normalization parameters

“Pitfalls” of Scattering Analysis

1. Data inconsistencies:

   i. Form factor slope
   ii. Form factor ratio

2. Radiative corrections needed to interpret lepton-scattering experiments

3. Model and extrapolation (to $Q^2 = 0$) uncertainty

i.

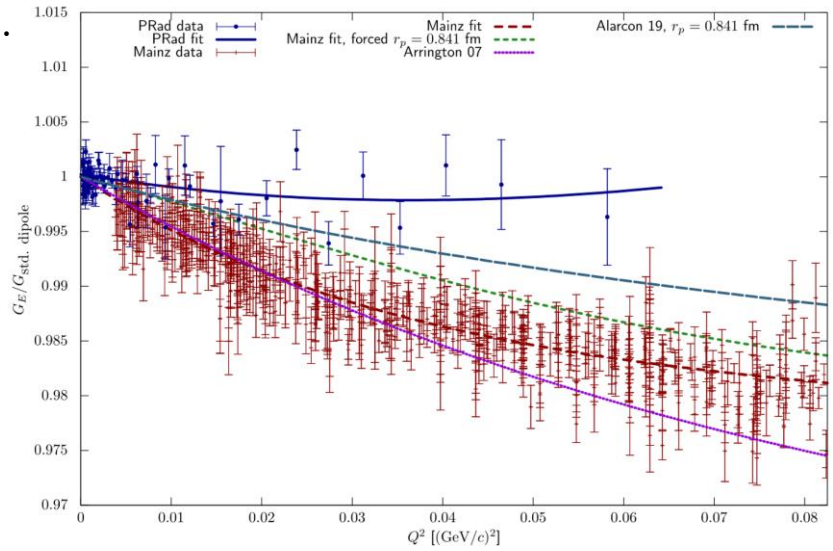

ii.

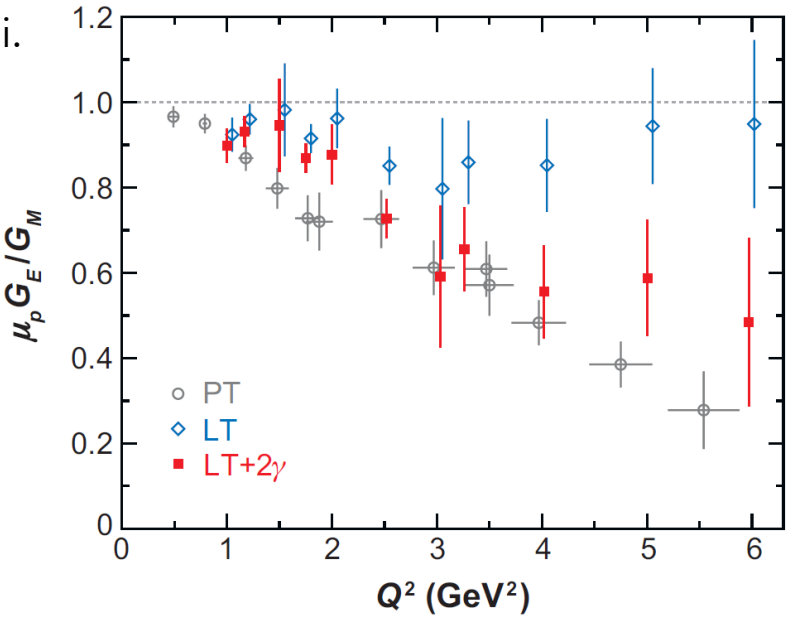

Lower Bound on Charge Radius

$$R_E^2(Q^2) = -\frac{6}{Q^2}\log G_E(Q^2) \overset{Q^2=0}{\longrightarrow} R_E^2$$

is a lower bound

$$R_E^2(Q^2) \leq R_E^2 \quad \text{for } Q^2 \geq 0$$

FH and V. Pascalutsa, Phys. Lett. B **797** (2019)

- $R_E^2(Q^2)$ is monotonically increasing towards $Q^2=0$
- Lower bound follows from finite Q^2 data, no extrapolation of FF data required

tentative evaluation: lower bound
from ISR and Bernauer data

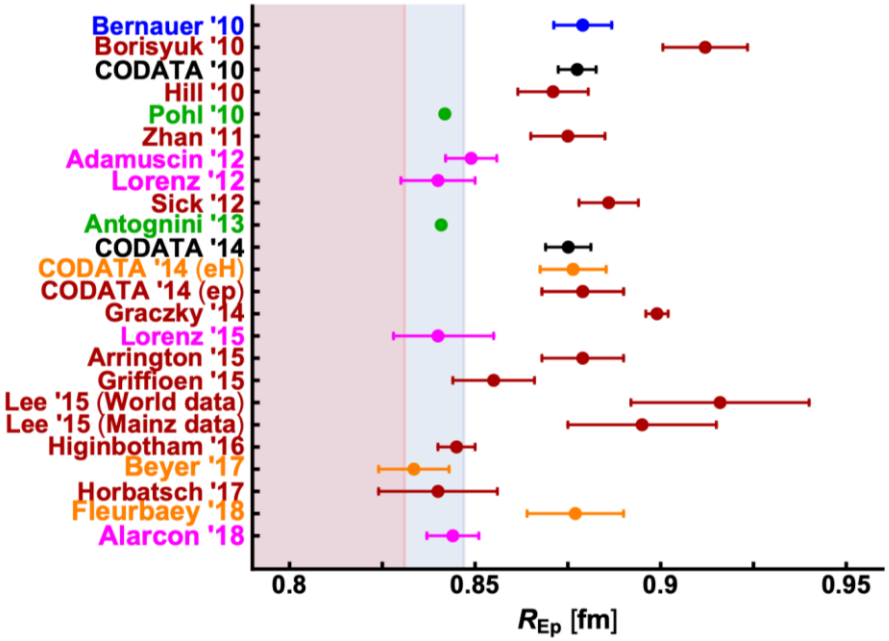

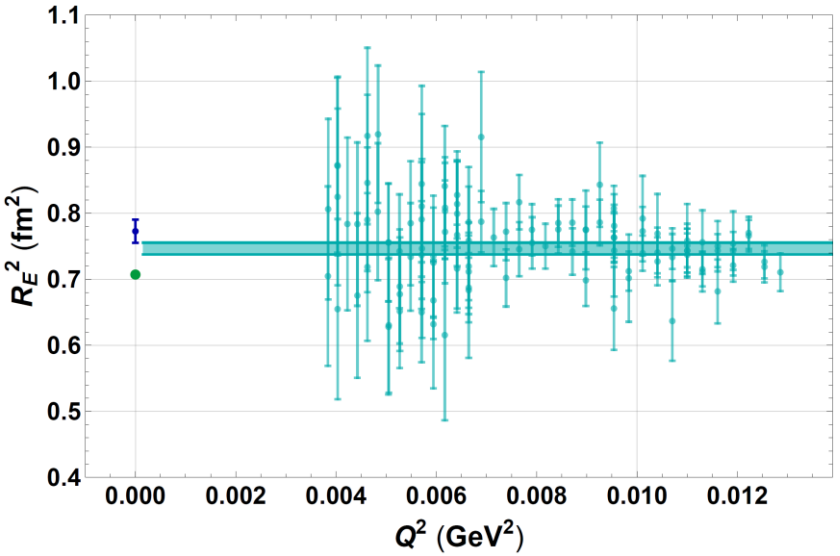

Finite-size Effects in HFS

$$\Delta E_{\rm HFS}(nS) = \left[1 + \Delta_{\rm QED} + \Delta_{\rm weak} + \Delta_{\rm structure}\right] E_F(nS)$$

with $\Delta_{\rm structure} = \Delta_Z + \Delta_{\rm recoil} + \Delta_{\rm pol}$

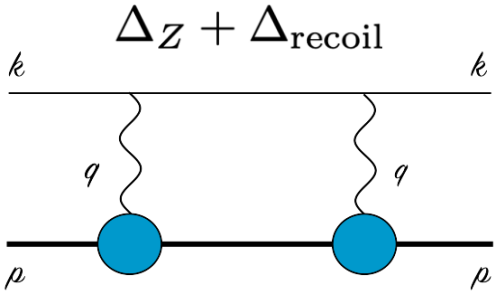

Zemach radius:

$$\Delta_Z = \frac{8Z\alpha m_r}{\pi}\int_0^\infty \frac{{\rm d}Q}{Q^2}\left[\frac{G_E(Q^2)G_M(Q^2)}{1+\kappa} - 1\right] \equiv -2Z\alpha m_r R_Z$$

experimental value: $R_Z = 1.082(37)\,{\rm fm}$

[Antognini, et al. '13]

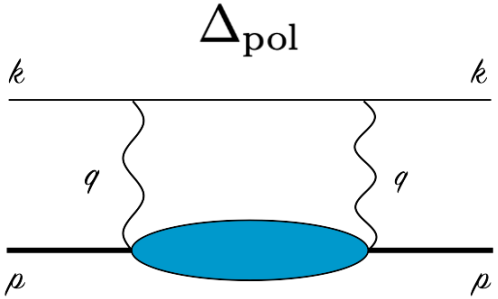

R_Z	Δ_Z	$\Delta_{\rm recoil}$	$\Delta_{\rm pol}$
$1.054^{+0.003}_{-0.002}$ fm	-7403^{+21}_{-16} ppm	850 ppm	37(95) ppm (LO BChPT)
[Lin, et al. '22]	[Antognini, et al. '22, annual reviews]	[Antognini, et al. '22]	[Hagelstein, et al. '23]

Zemach Radius Integrand Treatment

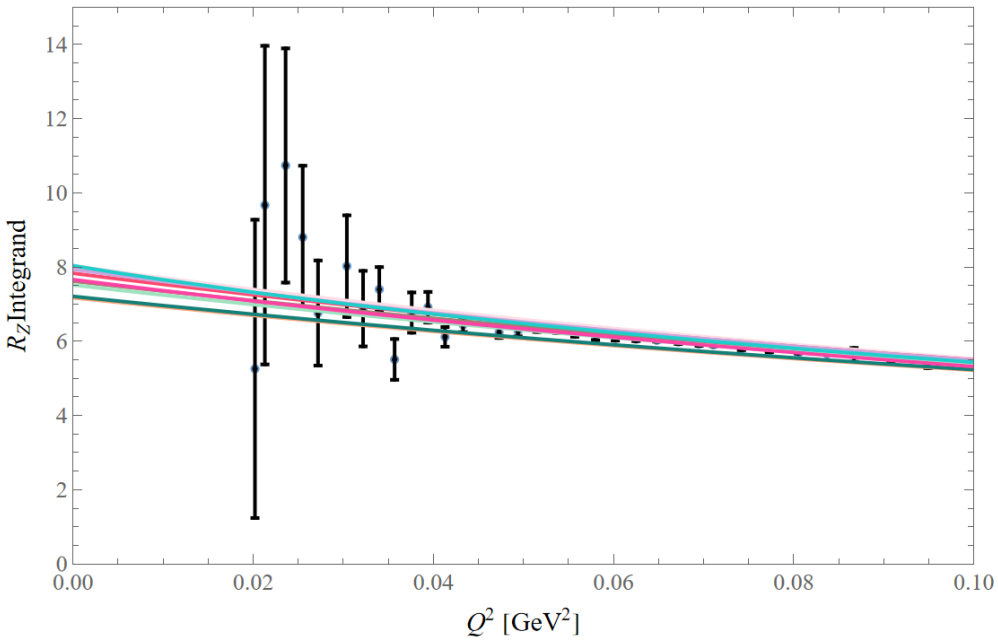

1. Use **Rosenbluth separation** data to remove model dependence from fitting cross sections
2. Splitting Q-region into three:
   i. Low-Q: no data
   ii. Medium-Q: direct data
   iii. High-Q: no data
3. Direct numerical integration over data
4. World data fit applied in regions i and iii

Stumbling stone: model-dependence in the low-Q region

IDEA!

Partial integration for the low-Q region to trade model-dependence and extrapolation uncertainty for data uncertainty

Partial Integration Trick for Zemach Radius

Initial integrand

$$R_Z = -\frac{4}{\pi}\int_0^\infty \frac{dQ}{Q^2}\left[\frac{G_E(Q^2)G_M(Q^2)}{1+\kappa}-1\right] = -\frac{2}{\pi}\int_0^\infty \frac{dQ^2}{Q^3}\left[\frac{G_E(Q^2)G_M(Q^2)}{1+\kappa}-1\right]$$

$$\int_0^{Q_0^2} dQ^2\, u(Q^2)v'(Q^2) = u(Q^2)v(Q^2)\Big|_0^{Q_0^2} - \int_0^{Q_0^2} dQ^2\, u'(Q^2)v(Q^2)$$

The optimal choice: smallest integral contribution

$$R_Z = \frac{4}{\pi}\int_0^{Q_0^2}\frac{dQ^2}{Q^3}\left\{1+\frac{Q^2\left[G_E(Q^2)G'_M(Q^2)+G_M(Q^2)G'_E(Q^2)\right]-G_E(Q^2)G_M(Q^2)}{1+\kappa}\right\}$$
$$+\frac{4}{\pi\,Q_0}\left(1-\frac{G_E(Q_0^2)\,G_M(Q_0^2)}{1+\kappa}\right)-\frac{2}{\pi}\int_{Q_0^2}^\infty\frac{dQ^2}{Q^3}\left[\frac{G_E(Q^2)G_M(Q^2)}{1+\kappa}-1\right]$$

Optimal Q_0 and Uncertainty Comparison

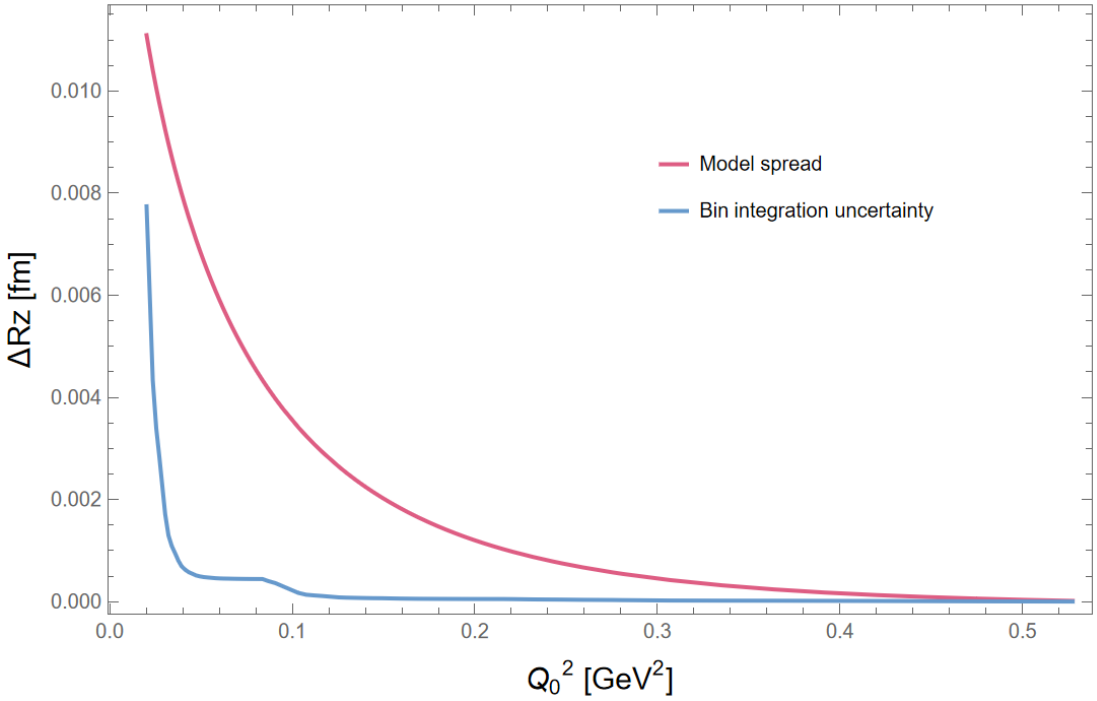

- Both uncertainties depend on the "stitching" point Q_0
- Model-dependence dominates the bin integration uncertainty
- Our Q_0 choice depends on the uncertainty of the surface term:

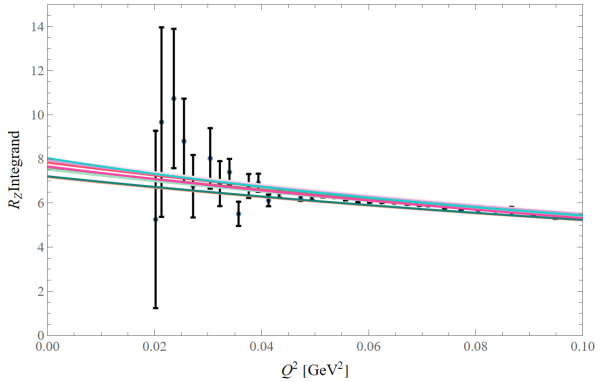

Future strategy:

1. Taking a set of different Q_0 that do not exceed a fixed error budget
2. Checking the consistency of each Q_0 choice (do results agree within uncertainty?)
3. Averaging over the results

Improved Zemach Radius Uncertainty

Q0 [GeV^2]	0 to Q0	Surface term (at Q0)	Q0 to Q1	Q1 to Infinity	Total
0.0413 Constraint: RE=0.84087 fm	0.02659 0.00200 model ±0.00346 model+fit	0.24533 ±0.01021 data	0.42726 ±0.00063 data ±0.00005 num	0.33804 constant -0.00535 ff ±0.00021 fit	**1.03188** ±0.00350 model+fit ±0.01023 data+num = **1.03188** ±**0.01080** total
	Total of 0 to Q0 0.27192				

PRELIMINARY

Q0	0 to Q0	Q0 to Q1	Q1 to Infinity	Total
0.0413 Constraint: RE=0.84087 fm	0.28320 central ±0.00850 model ±0.01010 fit+model	0.42530 central ±0.00157 model ±0.00199 model+fit	[0.33804 -0.00535] central ±0.00021 fit	**1.04119** central ±**0.01115** total

Correlation of Zemach and Charge, Magnetic Radii

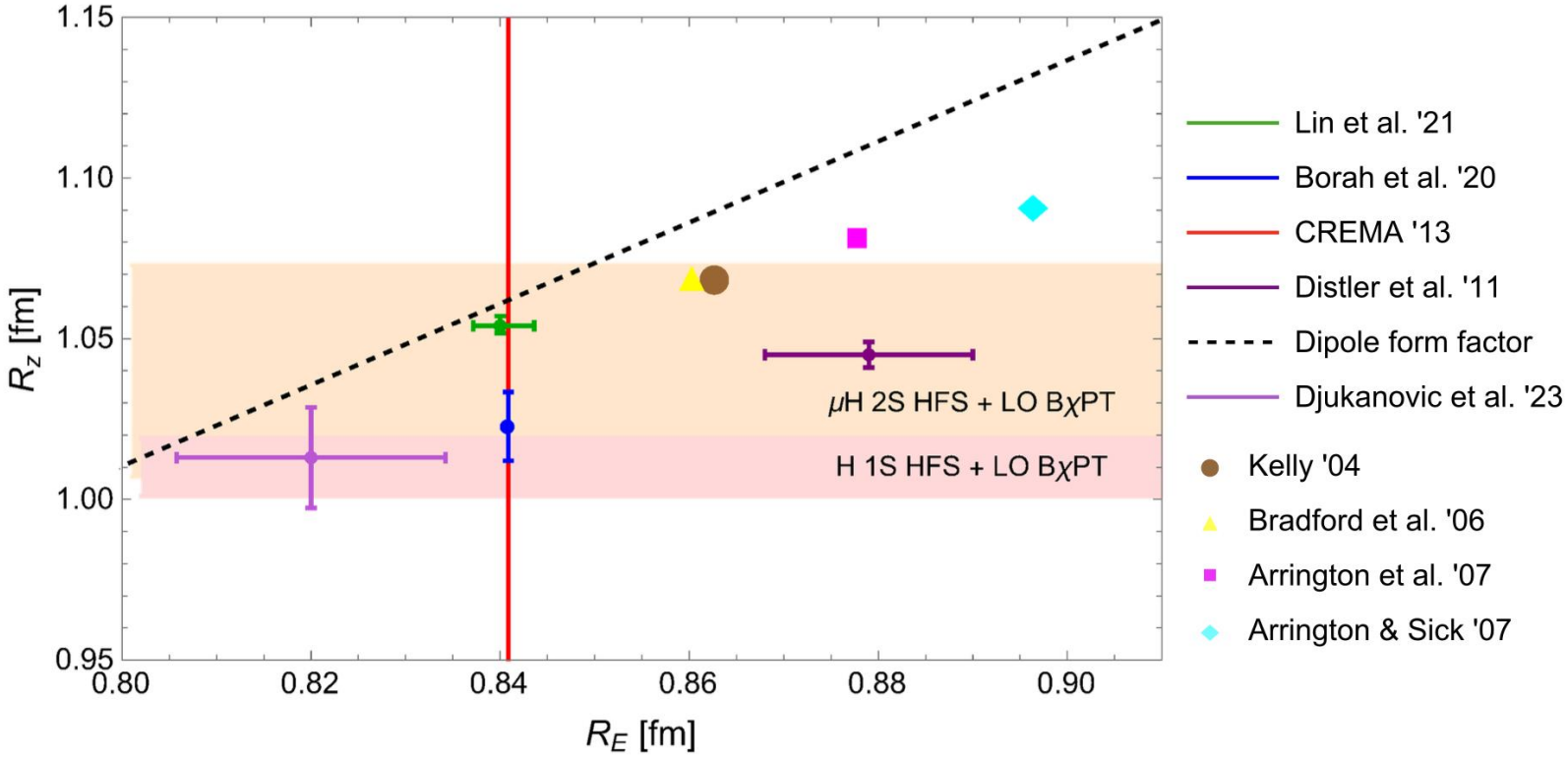

Zemach radius

$$R_Z \equiv -\frac{4}{\pi}\int_0^\infty \frac{dQ}{Q^2}\left[\frac{G_E(Q^2)G_M(Q^2)}{1+\kappa} - 1\right]$$

Friar Radius in μH Lamb Shift

- Elastic TPE splits into Friar radius + recoil part
  - Recoil is small for µH ~ 0.03(5) µeV [Karshenboim et al., PRD 91 (2015) 073003]
  - $E_{2S}^{\mathrm{el}} = -21.1(2)\,\mu\,\mathrm{eV}$ based on $R_F^3 = 2.310(26)\ \mathrm{fm}^3$]Lin et al. (2022), PRL]
- Aim: self-consistent extraction of R_E from spectroscopy [Karshenboim, PRD 90 (2014) 053012]

compare to future exp. uncertainty ~ 0.4 µeV

Table 1 Forward 2γ-exchange contributions to the $2S$ shift in muonic hydrogen (µeV)

Reference	$E_{2S}^{(\mathrm{subt})}$	$E_{2S}^{(\mathrm{inel})}$	$E_{2S}^{(\mathrm{pol})}$	$E_{2S}^{(\mathrm{el})}$	$E_{2S}^{(2\gamma)}$
Data-driven dispersive evaluation					
Pachucki 1999 (75)	1.9	−13.9	−12(2)	−23.2(1.0)	−35.2(2.2)
Martynenko 2006 (76)	2.3	−16.1	−13.8(2.9)		
Carlson et al. 2011 (77)	5.3(1.9)	−12.7(5)	−7.4(2.0)		
Birse & McGovern 2012 (78)	4.2(1.0)	−12.7(5)	−8.5(1.1)	−24.7(1.6)	−33(2)
Gorchtein et al. 2013 (79)[a]	−2.3(4.6)	−13.0(6)	−15.3(4.6)	−24.5(1.2)	−39.8(4.8)
Hill & Paz 2017 (80)					−30(13)
Tomalak 2019 (81)	2.3(1.3)		−10.3(1.4)	−18.6(1.6)	−29.0(2.1)
Leading-order baryon chiral perturbation theory					
Alarcón et al. 2014 (82)			$-9.6^{+1.4}_{-2.9}$		
Lensky et al. 2018 (83)[b]	$3.5^{+0.5}_{-1.9}$	−12.1(1.8)	$-8.6^{+1.3}_{-5.2}$		
Lattice QCD					
Fu et al. 2022 (84)					−37.4(4.9)

← used Karshenboim 2014

Self-consistent Charge Radius Extraction

Lamb Shift

$$E(2p_{1/2} - 2s_{1/2}) = \left(206.0573(45)_{\text{QED}} - 5.2262 r_p^2\right) \text{meV} + \frac{(Z\alpha)^5 m_r^4}{24} \langle r^3 \rangle_{E(2)} + E_{\text{pol.}}$$

charge radius

Friar radius

$$\langle r^3 \rangle_{E(2)} = \frac{24}{\pi} \int_0^\infty \frac{\mathrm{d}Q^2}{Q^5} \left[G_E^2(Q^2) - 1 + \frac{1}{3} R_E^2 Q^2 \right]$$

depends on charge radius

Our approach:

Importance of self-consistent extraction pointed out by [Karshenboim '14]

1. Splitting into low-Q, medium-Q and high-Q region
2. Directly integrating over the Rosenbluth form factor data
3. Using the World data fit for the low-Q and high-Q regions with the charge radius constraint
4. Obtaining Friar radius and theor. Lamb shift as a function of charge radius
5. Finding R_E for which exp. and theor. Lamb shift agree within uncertainties
6. Extraction R_E (band, w/o central value)

Correlation of Friar and Charge Radii

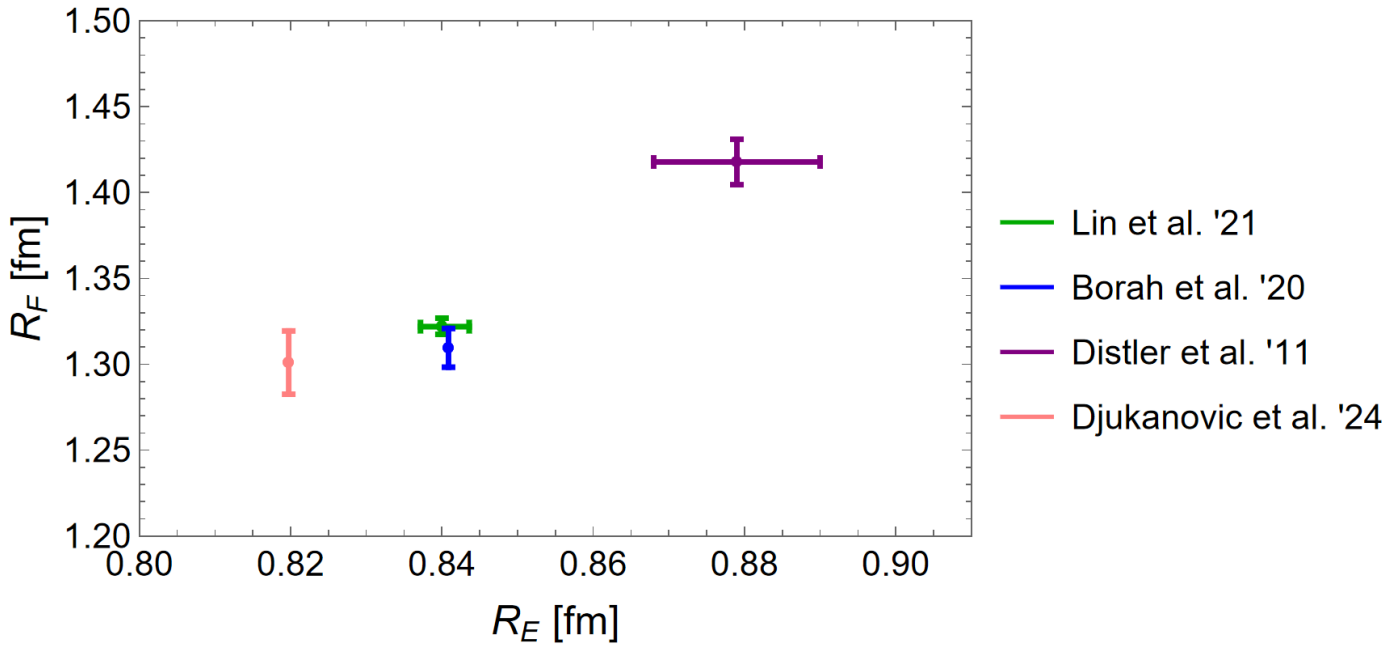

Friar radius or 3rd Zemach moment

$$R_{\rm F} = \sqrt[3]{\langle r^3 \rangle_{E(2)}},$$

$$\langle r^3 \rangle_{E(2)} \equiv \int {\rm d}\boldsymbol{r}\, r^3\, \varrho_{E(2)}(r), \quad \text{with} \quad \varrho_{E(2)}(r) = \int {\rm d}\boldsymbol{r}'\, \varrho_E(|\boldsymbol{r}' - \boldsymbol{r}|)\, \varrho_E(\boldsymbol{r}'),$$

$$\equiv \frac{48}{\pi} \int_0^\infty \frac{{\rm d}Q}{Q^4} \left[G_E^2(Q^2) - 1 + \tfrac{1}{3} R_E^2\, Q^2 \right];$$

charge radius

Partial Integration Trick for Friar Radius

Initial integrand

$$\langle r^3\rangle_{E(2)} = \frac{48}{\pi}\int_0^\infty \frac{\mathrm{d}Q}{Q^4}\left[G_E^2(Q^2) - 1 - 2\,G_E'(0)\,G_E(0)\,Q^2\right] = \frac{24}{\pi}\int_0^\infty \frac{\mathrm{d}Q^2}{Q^5}\left[G_E^2(Q^2) - 1 + \frac{1}{3}R_E^2 Q^2\right]$$

$$\int_0^{Q_0^2} \mathrm{d}Q^2\, u(Q^2)v'(Q^2) = u(Q^2)v(Q^2)\Big|_0^{Q_0^2} - \int_0^{Q_0^2} \mathrm{d}Q^2\, u'(Q^2)v(Q^2)$$

The optimal choice: smallest integral contribution

$$\langle r^3\rangle_{E(2)} = \frac{96}{\pi}\int_0^{Q_0^2} \frac{\mathrm{d}Q^2}{Q^5}\left\{G_E^2(Q^2) - 1 - Q^2 G_E(Q^2)G_E'(Q^2) + \frac{1}{6}Q^2R_E^2\right\} + \frac{48}{\pi\,Q_0^3}\left[G_E^2(Q_0^2) - 1 + \frac{1}{3}R_E^2Q_0^2\right] + \frac{24}{\pi}\int_{Q_0^2}^\infty \frac{\mathrm{d}Q^2}{Q^5}\left[G_E^2(Q^2) - 1 + \frac{1}{3}R_E^2Q^2\right]$$

Lower Bound on Magnetic Radius

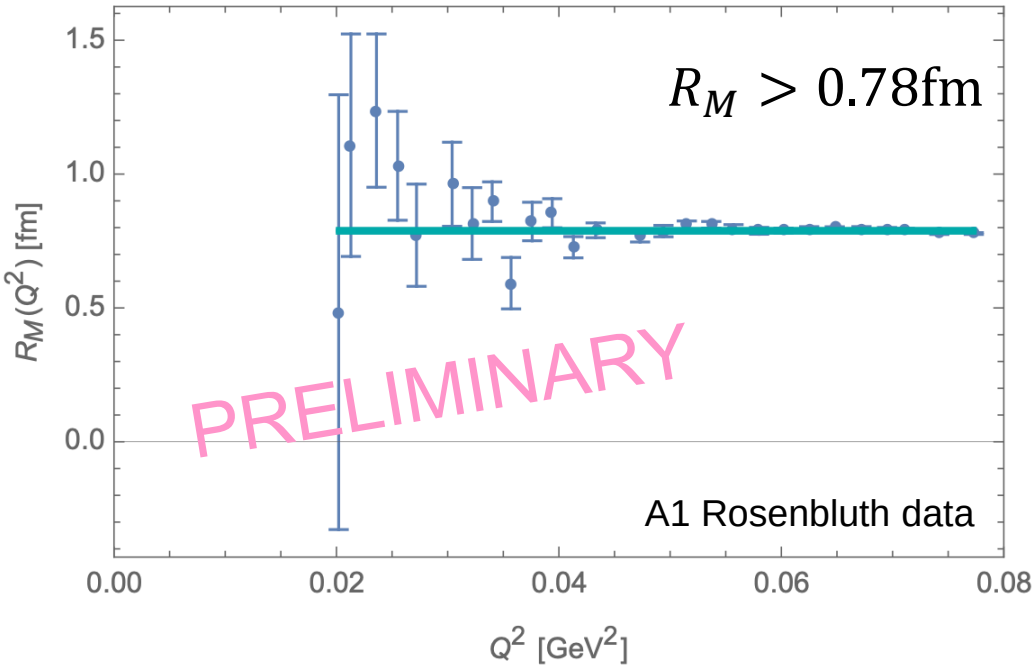

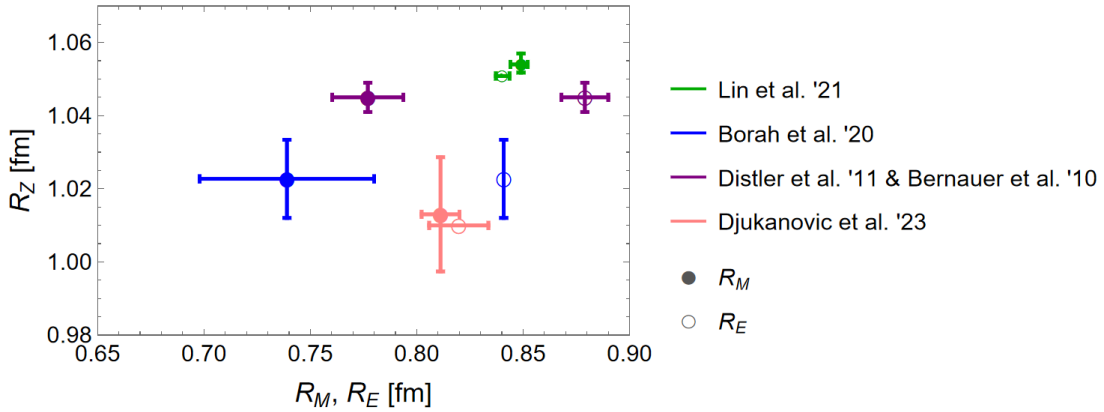

Magnetic Radius from Inelastic Scattering

- Burkhardt-Cottingham sum rule relates elastic form factors to the zeroth moment of an inelastic spin structure function:

$$I_2(Q^2) = \frac{2M^2}{Q^2}\int_0^{x_0} \mathrm{d}x\, g_2(x, Q^2) = \frac{1}{4} F_2(Q^2) G_M(Q^2)$$

- Constrain the magnetic radius through inelastic scattering:

$$R_M = \left[\frac{1}{1+2\kappa}\left(-\frac{24 I_2'(0)}{1+\kappa} - \frac{3\kappa}{2M^2} + \langle r^2 \rangle_E\right)\right]^{1/2}$$

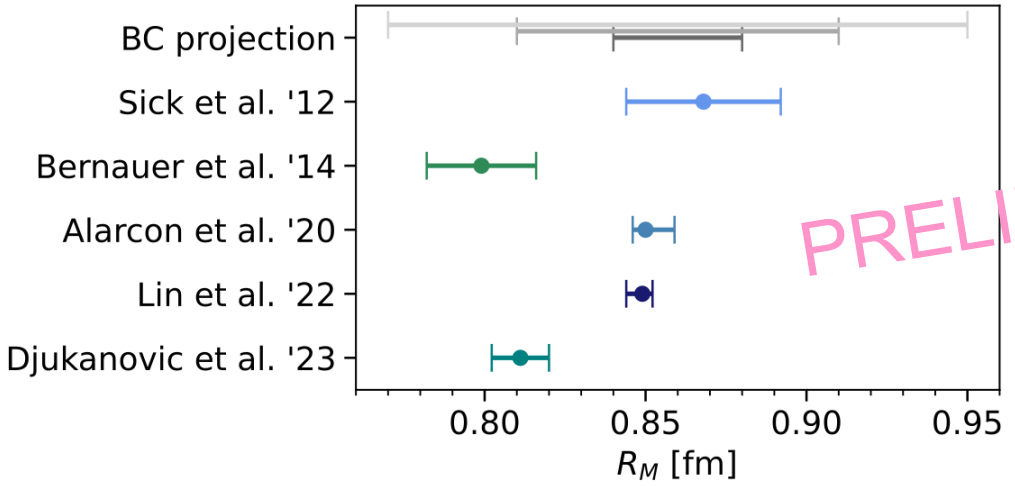

Projection assuming 25 %, 15 % and 5 % relative uncertainty for $I_2'(0)$

PRELIMINARY

Outlook and Conclusions

- Word of caution against optimistic view of uncertainties in extraction of proton radii from scattering

  i. Guidance of resonance search in muonic hydrogen 1S HFS

- Direct use of Rosenbluth extracted form factor data

  i. Lower bound on R_E and R_M
  ii. Numerical integration in R_Z and R_F

- Proton structure radii and TPE corrections in muonic atoms are dominated by low-Q

- Partial integration trick:

  i. Shifting the integrand weighting towards the date region
  ii. Trading model and extrapolation uncertainty for data uncertainty (surface term)

- Self-consistent extraction of R_E from muonic hydrogen LS

  i. Determine R_F as a function of R_E

Thank you for
your attention!

BACKUP

Self-consistent Charge Radius Extraction

3rd Zemach moment

$$\langle r^3 \rangle_2 = \frac{48}{\pi} I_3^{\mathrm{E}} \quad \text{with} \quad I_3^{\mathrm{E}} \equiv \int_0^\infty \frac{dq}{q^4} \left[\left(G_E(q^2) \right)^2 - 1 - 2G'_E(0)\, q^2 \right]$$

Splitting the integral at *q0* into two regions and treating them separately

$$I = \int_0^\infty dq... \equiv I_< + I_> \equiv \int_0^{q_0} dq... + \int_{q_0}^\infty dq...$$

$$I_{3<}^{\mathrm{E}} \equiv \int_0^{q_0} \frac{dq}{q^4} \left[\left(G_E(q^2) \right)^2 - 1 - 2G'_E(0)\, q^2 \right] \qquad I_{3>}^{\mathrm{E}} = \int_{q_0}^\infty \frac{dq}{q^4} \left[\left(G_E(q^2) \right)^2 - 1 - 2G'_E(0)\, q^2 \right]$$

Expanding the form factor for exact cancellation

$$\left(G_E(q^2) \right)^2 = A + Bq^2 + Cq^4 + ...$$

Model

$$A = 1 \qquad B = -R_E^2/3 \qquad C = C^{\mathrm{dip}} \times (1 \pm 1)$$

Integration over data

$$I_{3>}^{\mathrm{E}} \equiv I_{3>}^{\mathrm{E}}(\mathrm{data}) + \frac{1}{3} R_E^2 \int_{q_0}^\infty \frac{dq}{q^2}$$

charge radius

[Karshenboim, '14]

Finding an Optimal P.I. Weighting

$$R_Z = -\frac{4}{\pi}\int_0^\infty \frac{\mathrm{d}Q}{Q^2}\left[\frac{G_E(Q^2)G_M(Q^2)}{1+\kappa}-1\right] = -\frac{2}{\pi}\int_0^\infty \frac{\mathrm{d}Q^2}{Q^3}\left[\frac{G_E(Q^2)G_M(Q^2)}{1+\kappa}-1\right]$$

$$\int_0^{Q_0^2} \mathrm{d}Q^2\, u(Q^2)v'(Q^2) = u(Q^2)v(Q^2)\Big|_0^{Q_0^2} - \int_0^{Q_0^2} \mathrm{d}Q^2\, u'(Q^2)v(Q^2)$$

Low-Q expansion shows that the remaining integral is the smallest

$$-\frac{2}{\pi}\int_0^{Q_0^2}\frac{\mathrm{d}Q^2}{Q^3}\left[\frac{G_E(Q^2)G_M(Q^2)}{G_M(0)G_E(0)}-1\right] = -\frac{2}{\pi}\int_0^{Q_0^2}\frac{\mathrm{d}Q^2}{Q}\left[\frac{G_M(0)G'_E(0)+G_E(0)G'_M(0)}{G_M(0)G_E(0)}+\mathcal{O}(Q^2)\right]$$

Optimal choice

$$u(Q^2) = -\frac{2}{\pi}\frac{1}{Q^2}\left[\frac{G_E(Q^2)G_M(Q^2)}{1+\kappa}-1\right] \qquad v'(Q^2) = \frac{1}{\sqrt{Q^2}}$$

Uncertainty dependence on Qmax